

Research Article

Fabrication of CuO_x -Pd Nanocatalyst Supported on a Glassy Carbon Electrode for Enhanced Formic Acid Electro-Oxidation

Islam M. Al-Akraa ¹, Ahmad M. Mohammad ², Mohamed S. El-Deab ²
and Bahgat E. El-Anadouli²

¹Department of Chemical Engineering, Faculty of Engineering, The British University in Egypt, Cairo 11837, Egypt

²Chemistry Department, Faculty of Science, Cairo University, Cairo 12613, Egypt

Correspondence should be addressed to Ahmad M. Mohammad; ammohammad@cu.edu.eg and Mohamed S. El-Deab; msaada68@yahoo.com

Received 27 August 2018; Revised 17 October 2018; Accepted 13 November 2018; Published 2 December 2018

Guest Editor: Abdellatif Ait Lahcen

Copyright © 2018 Islam M. Al-Akraa et al. This is an open access article distributed under the Creative Commons Attribution License, which permits unrestricted use, distribution, and reproduction in any medium, provided the original work is properly cited.

Formic acid (FA) electro-oxidation (FAO) was investigated at a binary catalyst composed of palladium nanoparticles (PdNPs) and copper oxide nanowires (CuO_x NWs) and assembled onto a glassy carbon (GC) electrode. The deposition sequence of PdNPs and CuO_x NWs was properly adjusted in such a way that could improve the electrocatalytic activity and stability of the electrode toward FAO. Several techniques including cyclic voltammetry, chronoamperometry, field-emission scanning electron microscopy, energy dispersive X-ray spectroscopy, and X-ray diffraction were all combined to report the catalyst's activity and to evaluate its morphology, composition, and structure. The highest catalytic activity and stability were obtained at the CuO_x /Pd/GC electrode (with PdNPs directly deposited onto the GC electrode followed by CuO_x NWs with a surface coverage, Γ , of ca. 49%). Such enhancement was inferred from the increase in the peak current of direct FAO (by ca. 1.5 fold) which associated a favorable negative shift in its onset potential (by ca. 30 mV). The enhanced electrocatalytic activity and stability (decreasing the loss of active material by ca. 1.5-fold) of the CuO_x /Pd/GC electrode was believed originating both from facilitating the direct oxidation (decreasing the time needed to oxidize a complete monolayer of FA, increasing turnover frequency, by ca. 2.5-fold) and minimizing the poisoning impact (by ca. 71.5%) at the electrode surface during FAO.

1. Introduction

The growing petition for a clean fuel and the awareness of environmental problems have drawn the attention of the global community to substitute fossil fuels with other sources of clean energy [1, 2]. Of these, fuel cells were encouraging as they have been verified competent, consistent, sustainable, noiseless, long-lasting, and simply installed and moved; hence, they were excellent for transportation and suburban uses as well as portable electronics [3–7]. To date, the direct formic acid fuel cells (DFAFCs) have shown more preferred than hydrogen fuel cells (HFCs) and direct methanol fuel cells (DMFCs) in providing electricity for portable electronics [6–14]. In fact, the transportation and storage of formic acid (FA, the energy carrier in DFAFCs)

was much easier than H_2 , and it could exhibit, moreover, a lower crossover than methanol through Nafion-based membranes. This permitted a higher practical energy density because of allowing the usage of thinner membranes and more concentrated fuel solutions [15, 16]. In addition, FA can be sustainably manufactured by CO_2 electrochemical reduction utilizing excess clean electrical power sources such as solar farms and wind turbines [17].

With the revolution of nanotechnology, several nanostructures have been recommended for applications of multidiversity [18–21]. Platinum-based catalysts have been commonly used as for the electro-oxidation of formic acid (FAO) [22, 23]. On Pt-based materials, FAO proceeded in two pathways at the same time: the direct (favorable—in which FA is converted to CO_2 at a low anodic potential)

[9, 15–17] and the indirect (unfavorable—in which FA is converted to poisoning CO that is then oxidized at higher potentials by platinum hydroxide species) [24]. Unluckily, CO adsorption in the low potential domain at the Pt surface deactivated its catalytic activity, which finally impeded the direct pathway of FAO [24–26]. Scheme 1 represents the dehydrogenation and dehydration pathways of FAO at Pt surfaces.

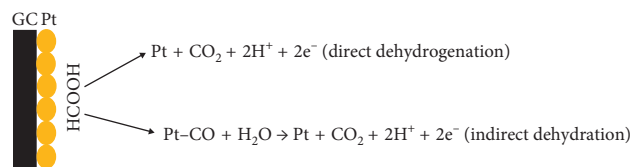
Compared with Pt, Pd can catalyze the FAO through a more facile direct path to produce CO₂ with less vulnerability to CO poisoning [27, 28]. However, Pd-based catalysts used to be subjected to a potential deactivation with time that originated typically from the adsorption of some CO-like poisoning species [29, 30]. The catalytic performance of Pd catalysts toward FAO was recently enhanced by doping with other metals and/or metal oxides that have the capacity to reduce the adsorption of these poisoning intermediates [31–34]. In the previous study [12], MnO_x was able to enhance the electrocatalytic performance of Pd in such a way that minimized the adsorption of poisoning species depicted from calculating the long-term poisoning rate (δ). This modification reduced δ to 0.11, 0.08, and 0.05%·s⁻¹ at the Pd/MnO_x/GC, MnO_x/Pd/GC, and Pd-MnO_x/GC electrodes, respectively.

Doping platinum and palladium with nonprecious copper or copper oxide has not only exhibited outstanding improvement in the catalytic activities and stability of several potential electrochemical reactions [35–38], but also it offers a very effective way that could reduce the loading of noble metals. Hence, a motivation to report on the enhanced efficiency of a CuO_x/Pd/GC nanocatalyst (in which PdNPs was directly electrodeposited onto a GC surface followed by CuO_xNWs) toward FAO exists. The electrodeposition technique is utilized as it attracted particular attention due to the ease of preparation, suitability for special-shaped electrodes, and low-cost requirement. The influence of deposition sequence and loading level of CuO_xNWs was examined to maximize the catalytic performance toward FAO.

2. Experimental

2.1. Electrochemical Measurements. After cleaning with conventional procedures, the electrode was mechanically polished with No. 2000 emery paper and then with aqueous slurries of successively finer alumina powder (down to 0.06 μm) with the help of a polishing microcloth. Next, the polished electrode was rinsed thoroughly with distilled water, and glassy carbon (GC, $d = 3.0$ mm) electrode was served as a working electrode. A spiral Pt wire and an Ag/AgCl/KCl (sat.) were used as counter and reference electrodes, respectively. All potentials in this investigation were measured in reference to Ag/AgCl/KCl (sat.).

The electrochemical measurements were performed at room temperature (25 ± 1 °C) in a two-compartment three-electrode glass cell. The measurements were performed using EG&G potentiostat (model 273A). Current densities were calculated on the basis of the real surface area of the working electrodes. The electrocatalytic activity of the



SCHEME 1: Dehydrogenation and dehydration pathways of FAO.

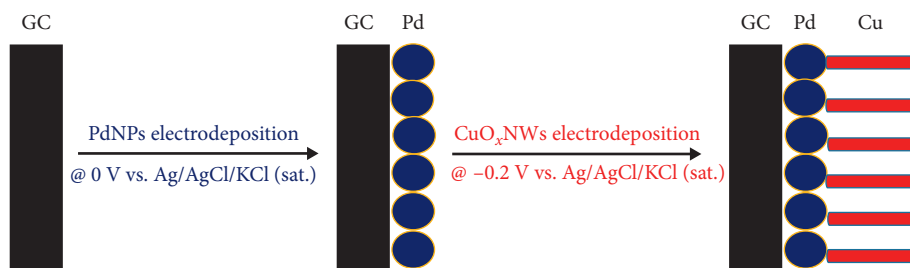
modified electrodes toward FAO was examined in an aqueous solution of 0.3 M FA solution (pH = 3.5, pH was adjusted by adding a proper amount of NaOH) at a scan rate of 100 mV·s⁻¹ (first cycle is recorded). At this pH, the polarization resistance will be reduced, thus the solution ionic conductivity was enhanced [39].

2.2. Electrodeposition of PdNPs and CuO_xNWs. The electrodeposition of PdNPs was carried out in 0.1 M H₂SO₄ solution containing 1.0 mM Pd(CH₃COO)₂ at a constant potential electrolysis at 0 V for 300 s. The PdNPs loading was estimated from Faraday's law using the charge associated in the i - t curve obtained during deposition to be ca. 18 μg·cm⁻². Alternatively, the electrode's modification with CuO_xNWs was carried out in 0.1 M H₂SO₄ solution containing 1.0 mM CuSO₄ at a constant potential electrolysis at -0.2 V for various durations [38]. These durations were set to control the amount of the electrodeposited Cu. The experimental protocol used for the surface modification of GC electrode with PdNPs and CuNWs is shown in Scheme 2.

2.3. Materials Characterization. A field-emission scanning electron microscope, FE-SEM, (QUANTA FEG 250) coupled with an energy dispersive X-ray spectrometer (EDS) was served to determine the morphology and composition of the investigated electrodes. An X-ray diffraction (XRD, PANalytical, X'Pert PRO) operated with Cu target ($\lambda = 1.54$ Å) revealed the crystallographic structure of the modified catalysts. The inductively coupled plasma optical emission spectrometry, ICP-OES, (Perkin Elmer, Optima 8000) has been utilized to specify if there was a loss in the catalysts' materials (Pd&Cu) after the prolonged electrolysis and to determine the amounts lost.

3. Results and Discussion

3.1. Electrochemical and Materials Characterization. Cyclic voltammograms (CVs) for (a) Pd/GC, (b) CuO_x/GC, (c) Pd/CuO_x/GC, and (d) CuO_x/Pd/GC electrodes measured in 0.5 M H₂SO₄ are shown in Figure 1. Figure 1(a) depicts the characteristic response of Pd surfaces where its oxidation started between 0.6 and 1.2 V was combined with this oxide reduction at ca. 0.4 V [33]. Besides that, the peaks that appeared in the potential range from 0 to -0.2 V were assigned to the hydrogen adsorption/desorption (H_{ads/des}). For the CuO_x/GC electrode (Figure 1(b)), a main oxidation peak appeared at ca. 0.15 V coupled with a reduction peak after ca. 0 V corresponding to the CuO_x formation and reduction [27, 29]. After the deposition of PdNPs onto the



SCHEME 2: The experimental protocol used for the surface modification of GC electrode with PdNPs and CuNWs.

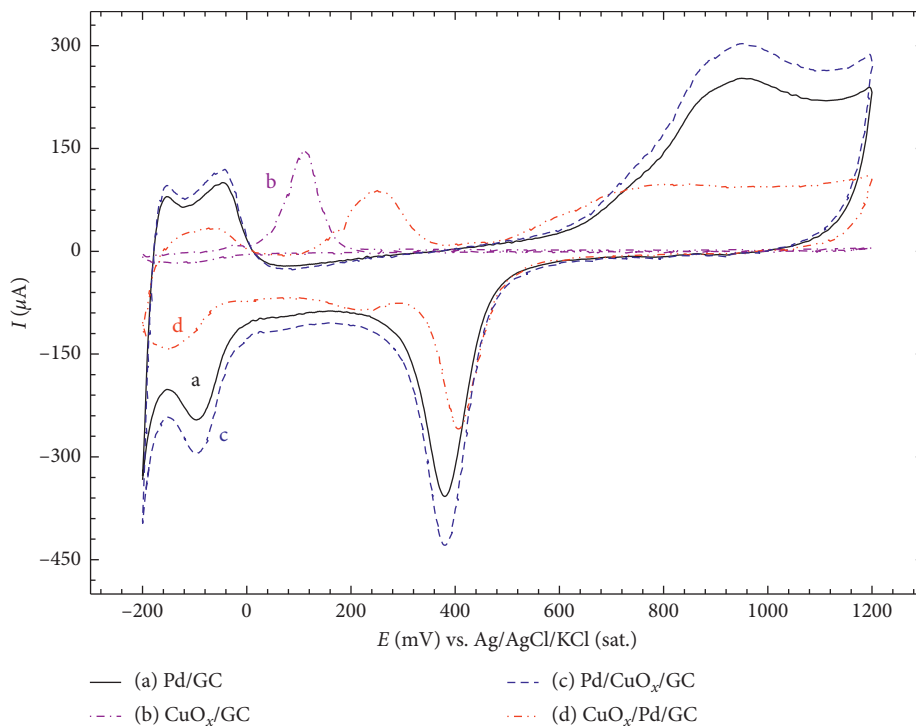


FIGURE 1: CVs obtained at (a) Pd/GC, (b) CuO_x/GC, (c) Pd/CuO_x/GC, and (d) CuO_x/Pd/GC electrodes in 0.5 M H₂SO₄. Potential scan rate: 100 mVs⁻¹.

CuO_x/GC electrode (Pd/CuO_x/GC electrode, Figure 1(c)), the intensity of the Pd oxide reduction peak increased coinciding with the increase in the intensity of the Pd oxide and the H_{ads/des} peaks. This is expected as the loading of CuO_xNWs on the GC surface can offer more active sites for the deposition of PdNPs; therefore, the Pd surface area could be seen increased. On the contrary, upon modifying the Pd/GC electrode with CuO_xNWs (Figure 1(d)), two new features were noticed:

- (i) A significant decrease in the intensities of the Pd oxide reduction and the H_{ads/des} peaks. This suggests a significant decrease in the PdNPs surface area as a result of CuO_xNWs deposition.
- (ii) A redox couple at ca. 0.25 V corresponding to the Cu oxidation and reduction [27–30].

These new features of the CuO_x/Pd/GC catalyst confirmed the surface exposure of both PdNPs and CuO_xNWs to the electrolyte.

Figure 2 displays FE-SEM images of the Pd/GC (Figure 2(a)), CuO_x/GC (Figure 2(b)), Pd/CuO_x/GC (Figure 2(c)), and CuO_x/Pd/GC (Figure 2(d)) electrodes. It illustrates that Pd was electrodeposited onto the GC electrode in a well-dispersed spherical lumps with an average particle size of ca. 75 nm (Figures 2(a), 2(c), and 2(d)), whereas CuO_x has been electrodeposited as hair-like nanowires (Figures 2(b) and 2(d)). The disappearance of the CuO_x morphology for the Pd/CuO_x/GC electrode (Figure 2(c)), in contrast to the case for CuO_x/Pd/GC (Figure 2(d)), infers that it has been covered during Pd deposition. This difference in morphology may affect the electrocatalytic parameters of FAO which will be displayed in the next section.

The EDS analysis of the Pd/GC, CuO_x/GC, and CuO_x/Pd/GC electrodes confirmed the deposition of the different ingredients in the catalyst and assisted in calculation of their relative ratios (Figures 3(a)–3(c)). Moreover, the crystal structure of the Pd/GC, CuO_x/GC, and CuO_x/Pd/GC electrodes was investigated utilizing the XRD technique.

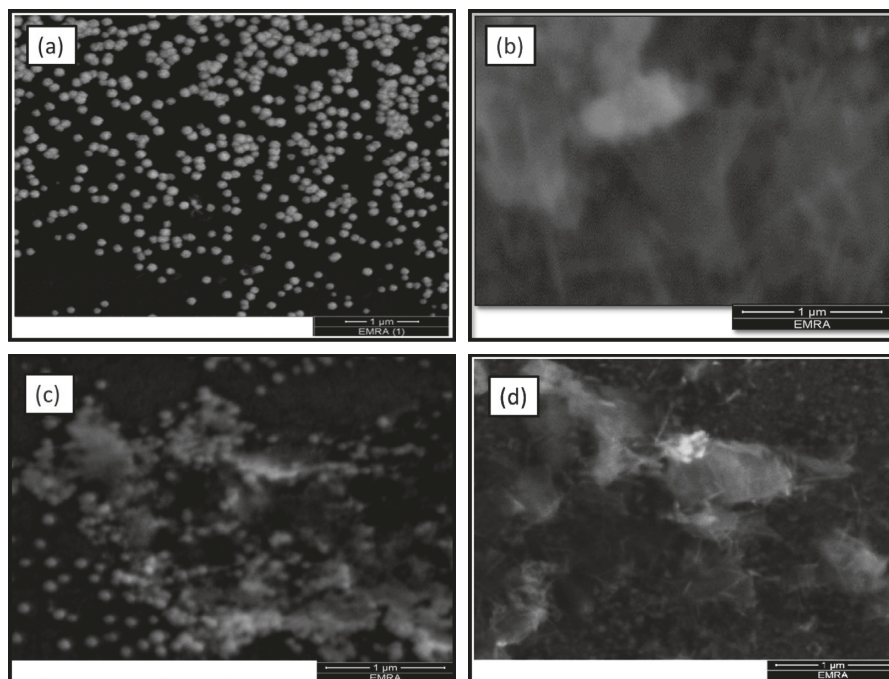


FIGURE 2: FE-SEM images of (a) Pd/GC, (b) CuO_x/GC, (c) Pd/CuO_x/GC, and (d) CuO_x/Pd/GC electrodes. The electrodeposition conditions are listed in the experimental section.

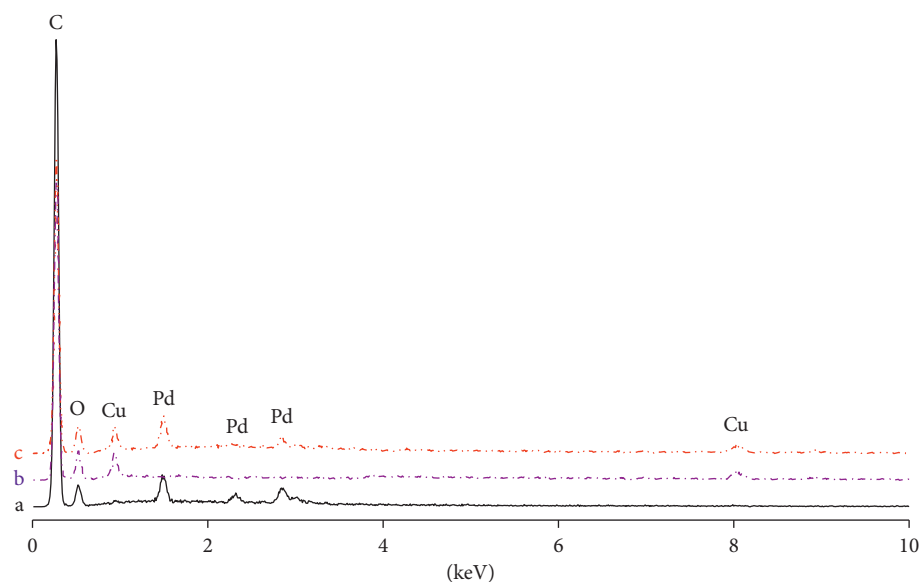


FIGURE 3: EDS analysis of (a) Pd/GC, (b) CuO_x/GC, and (c) CuO_x/Pd/GC electrodes. The electrodeposition conditions are listed in the experimental section.

In fact, the XRD analysis of the Pd/GC and CuO_x/Pd/GC electrodes (Figures 4(a) and 4(c)) displayed several diffraction peaks at ca. 39.7°, 43.2°, 67.2°, and 78° corresponding, respectively, to the (1 1 1), (2 0 0), (2 2 0), and (3 1 1) planes of Pd face-centered cubic (fcc) lattice [40, 41]. However, in Figures 4(b) and 4(c), a very small diffraction peak appeared at ca. 43.3° corresponding to Cu (1 1 1) plane. There were also two broad diffraction peaks for C (0 0 2) and (1 0 0) planes between 21–28° and 42–46°, respectively [42]. The C (1 0 0)

peak was much higher and broader than those of Pd (200) and Cu (111) and that is why they appeared like a single peak.

3.2. Electrocatalytic Activity toward FAO

3.2.1. Effect of Deposition Sequence. Figure 5 shows CVs of FAO at the Pd/GC, CuO_x/GC, Pd/CuO_x/GC, and CuO_x/Pd/GC electrodes in a 0.3 M aqueous solution of FA (pH = 3.5).

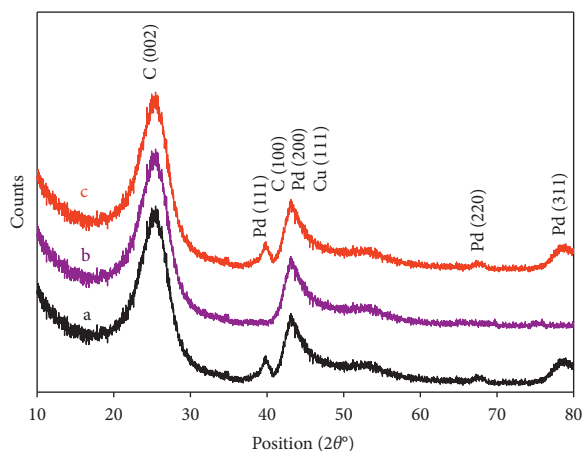


FIGURE 4: XRD patterns of (a) Pd/GC, (b) CuO_x/GC, and (c) CuO_x/Pd/GC electrodes. The electrodeposition conditions are listed in the experimental section.

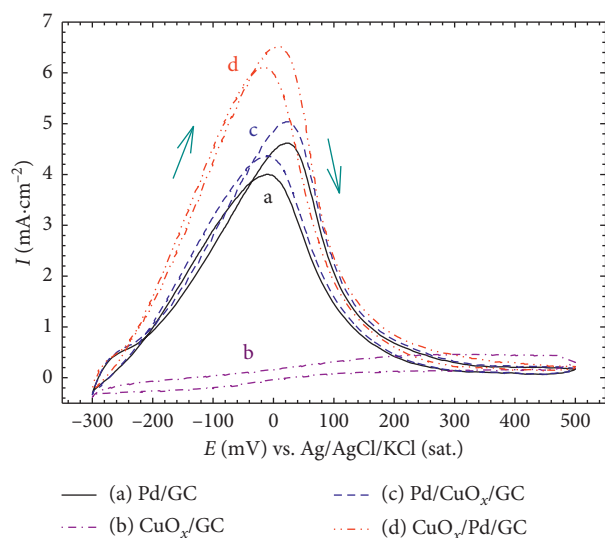


FIGURE 5: CVs obtained at (a) Pd/GC, (b) CuO_x/GC, (c) Pd/CuO_x/GC, and (d) CuO_x/Pd/GC electrodes in 0.3 M FA (pH = 3.5). Potential scan rate: 100 mV s⁻¹.

It is important to consider the inactivity of the unmodified GC electrode toward FAO [25, 43]. Inspection of Figure 5 reveals few interesting remarks:

- (i) The reaction pathway of FAO on the Pd/GC electrode (Figure 5(a)) proceeded exclusively via the dehydrogenation route in which CO₂ was the only oxidation product with insignificant contribution of Pd poisoning by CO [44, 45]. This was evident from the appearance of a single oxidation peak around ca. 0 V, which assigned the direct oxidation of FA to CO₂ [33].
- (ii) The electrodeposition of CuO_x directly at GC electrode surface did not show any activity for FAO (Figure 5(b)) to confirm the inertness of CuO_x as well as the GC substrate toward FAO.

- (iii) The deposition of PdNPs at GC electrode surface modified with CuO_x to obtain Pd/CuO_x/GC electrode (Figure 5(c)) a little bit shifts the current density of the oxidation peak (I_p) to a higher value as compared to the Pd/GC electrode (Figure 5(a)). This was likely because it had a higher surface area of PdNPs (as discussed before in Figure 1).
- (iv) The electrodeposition of CuO_xNWs at the GC electrode surface previously modified with PdNPs (Pd/GC) to obtain CuO_x/Pd/GC electrode (Figure 5(d)) exhibited an enhanced performance toward FAO with an increase of I_p (ca. 1.5 fold) and a negative shift (ca. 30 mV) in the onset potential (E_{onset}) of FAO. Recalling the smaller surface area of Pd in the CuO_x/Pd/GC electrode than in the Pd/GC electrode (compare Figures 1(a) and 1(d)), one may exclude the geometrical factor in the catalytic enhancement to suggest rather an electronic influence for CuO_xNWs that could presumably promote the charge transfer of the direct FAO at the electrode surface [17, 29, 46].

3.2.2. Effect of Loading Level of CuO_xNWs at Pd/GC Electrode. Optimization of the loading level of CuO_xNWs onto the Pd/GC electrode toward FAO has been investigated. A gradual decrease in the surface area of PdNPs reflected by a decrease in the intensity of the Pd oxide reduction and the H_{ads/des} peaks with the loading of CuO_xNWs have been observed. Table 1 summarizes the variation of the surface coverage (Γ) of CuO_xNWs electrodeposited onto the Pd/GC electrode with time and its effect on the peak current of FAO, I_p . As obviously seen, the I_p increased systematically to a certain value with Γ and then decreased. This makes sense as the catalytic activity of the CuO_x/Pd/GC electrode is expected to increase with the loading level of CuO_xNWs as long as the accessible surface area of PdNPs is sufficient to sustain the adsorption of FA. However, beyond certain coverage (ca. 49%), the accessible surface area of PdNPs becomes limiting in estimating the overall rate of FAO.

3.3. Stability of CuO_x/Pd/GC Electrode. Stability of the Pd-based catalysts is another important parameter in the practical use of DFAFCs. Figure 6 shows current transients of the Pd/GC, Pd/CuO_x/GC, and CuO_x/Pd/GC electrodes in a 0.3 M aqueous solution of FA (pH = 3.5) at -0.1 V. We did not include the data of the CuO_x/GC electrode as it did not show any activity toward FAO (Figures 5(b), 6(a), and 6(b)) (Pd/GC and Pd/CuO_x/GC electrodes, respectively) depicting a poor stability toward FAO, as can be obtained from the fast current drop with time, which agreed with other investigations in the literature [33, 46]. Interestingly, the CuO_x/Pd/GC electrode (Figure 6(c)) exhibited a higher current density in the activation polarization region, and its final current density was 1.6 mA·cm⁻² (compare it with 0.07 and 0.3 mA·cm⁻² obtained at the Pd/GC and Pd/CuO_x/GC electrodes). This may be assigned to the difference in the degree of poisoning of the three electrodes. The long-term

TABLE 1: Variation of the surface coverage (Γ) of CuO_x NWs electrodeposited onto Pd/GC electrode with deposition time and its effect on I_p of FAO.

Dep. time (min)	Real surface area (S) ^a (cm^2) CuO_x /Pd/GC	($\Gamma\%$) ^b	I_p ($\text{mA}\cdot\text{cm}^{-2}$)
0	0.49	0	4.5
1	0.38	22	5.2
2	0.25	49	6.5
3	0.17	65	5.9
4	0.10	80	5.4

^aAs estimated from the charge consumed during the reduction of the surface oxide monolayer in 0.5 M H_2SO_4 using a reported value of $420 \mu\text{C}\cdot\text{cm}^{-2}$. ^bThe values of surface coverage ($\Gamma = 1 - S_{\text{modified}}/S_{\text{unmodified}}$) were calculated for the various CuO_x /Pd/GC electrodes. S_{modified} and $S_{\text{unmodified}}$ refer to the real surface area of the modified and the unmodified Pd/GC electrodes, respectively.

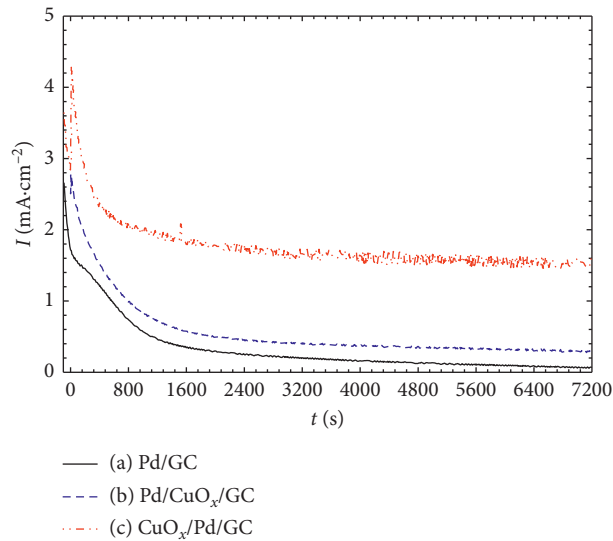


FIGURE 6: Current transients of (a) Pd/GC, (b) Pd/ CuO_x /GC, and (c) CuO_x /Pd/GC electrodes in 0.3 M FA (pH = 3.5) at -0.1 V.

poisoning rate (δ) could be calculated by measuring the linear decay of the current at intervals longer than 500 s using the following equation [47]:

$$\delta = \frac{100}{i_o} \times \left(\frac{di}{dt} \right)_{t > 500} \quad \% \cdot \text{s}^{-1}, \quad (1)$$

where $(di/dt)_{t > 500}$ is the slope of the linear portion of the current decay and i_o is the current at the start of polarization back-extrapolated from the linear current decay, respectively. Fascinatingly, the CuO_x /Pd/GC electrode showed a lower poisoning rate (ca. $0.002\% \cdot \text{s}^{-1}$) if compared to those obtained at both the Pd/GC (ca. $0.007\% \cdot \text{s}^{-1}$) and Pd/ CuO_x /GC electrodes (ca. $0.005\% \cdot \text{s}^{-1}$). This also infers about how CuO_x promoted FAO at the Pd- CuO_x modified catalysts.

Furthermore, some important electrocatalytic parameters, calculated from pseudosteady state current, such as time needed to oxidize a complete monolayer of FA and turnover frequency (TOF), have been estimated for the modified electrodes. Utilizing the charge associated with oxidation of a complete monolayer of FA, the complete oxidation of a FA monolayer at the Pd/GC and Pd/ CuO_x /GC electrodes, respectively, needed 0.86 and 0.82 s on the basis of a two-site adsorption model, and the corresponding TOF was estimated as 2.33 and 2.44 s^{-1} [48], respectively. Interestingly, based on

the same adsorption model, the complete oxidation of a FA monolayer at the CuO_x /Pd/GC electrode needed 0.35 s, and the corresponding TOF was 5.71 s^{-1} . These parameters could infer about the superior catalytic activity of the as-prepared CuO_x /Pd/GC electrode. Table 2 summarizes the electrochemical parameters, extracted from Figures 5 and 6, of the CuO_x /Pd/GC compared with Pd/GC and Pd/ CuO_x /GC electrodes. It also compares the data obtained in this investigation with the same data obtained from other previous investigations at which Pt surface was modified with nano- NiO_x and IrNPs [49, 50].

Further, the inductively coupled plasma optical emission spectrometry (ICP-OES) has been utilized to specify if there was a loss in the catalysts' materials (Pd and Cu) after the prolonged electrolysis and to determine the amounts lost. A minor loss was obtained after 2 h of electrolysis in FA. Importantly, the loss of the active material toward FAO (Pd) in the Pd/GC electrode was ca. 1.5 of that obtained at the modified CuO_x /Pd/GC electrode confirming once again the superiority of the CuO_x /Pd/GC electrode toward FAO (Table 3).

4. Conclusion

A novel binary catalyst composed of PdNPs and CuO_x NWs has been assembled onto the GC electrode for the efficient

TABLE 2: Electrochemical parameters, extracted from Figures 5 and 6, of the CuO_x/Pd/GC compared with Pd/GC, Pd/CuO_x/GC electrodes in this study and other previously reported catalysts.

Electrode	I_p (mA·cm ⁻²)	$I_E = 6$ mV/mA·cm ⁻²	E_{onset} (mV)	δ (%·s ⁻¹)	TOF (s ⁻¹)	References
Pd/GC	4.40	4.52	-230	0.007	2.33	This study
Pd/CuO _x /GC	5.00	4.93	-242	0.005	2.44	This study
CuO _x /Pd/GC	6.50	6.51	-260	0.002	5.71	This study
Pd/NiO _x /GC	5.20	5.29	-236	0.006	2.10	[49]
Pd/Ir/GC	3.30	3.25	-250	0.05	1.90	[50]

$I_E = 6$ mV: current density value at a same potential of 6 mV.

TABLE 3: Inductively coupled plasma optical emission spectrometry (ICP-OES) measured after 2 h of electrolysis in FA for CuO_x/Pd/GC and Pd/GC electrodes.

Analyte	Wavelength (nm)	Electrode	Conc (sample) (mg·L ⁻¹)
Pd	340.458	Pd/GC	0.032
		CuO _x /Pd/GC	0.021
Cu	324.752	CuO _x /Pd/GC	0.095

FAO. The deposition sequence of both PdNPs and CuO_xNWs onto the GC electrode influenced, to a great extent, the catalytic efficiency. The highest catalytic activity and stability were obtained at the CuO_x/Pd/GC electrode (in which CuO_xNWs were partially deposited, $\Gamma \approx 49\%$, onto the Pd/GC electrode). The enhancement in the electrocatalytic activity (increasing I_p of direct FAO by ca. 1.5-fold and decreasing E_{onset} by ca. 30 mV) and stability (decreasing both current decay and loss of active metal, by ca. 1.5-fold, during prolonged electrolysis) of the CuO_x/Pd/GC electrode was believed originating both from facilitating the direct oxidation of FA (increasing turnover frequency by ca. 2.5-fold) and minimizing the adsorption of poisoning species (by ca. 71.5%) at the electrode surface.

Data Availability

The data used to support the findings of this study are available from the corresponding author upon request.

Conflicts of Interest

The authors declare that there are no conflicts of interest regarding the publication of this paper.

References

- [1] M. Carmo, G. Doubek, R. C. Sekol, M. Linardi, and A. D. Taylor, "Development and electrochemical studies of membrane electrode assemblies for polymer electrolyte alkaline fuel cells using FAA membrane and ionomer," *Journal of Power Sources*, vol. 230, pp. 169–175, 2013.
- [2] S. Nishimura, N. Ikeda, and K. Ebitani, "Selective hydrogenation of biomass-derived 5-hydroxymethylfurfural (HMF) to 2,5-dimethyl furfural (DMF) under atmospheric hydrogen pressure over carbon supported PdAu bimetallic catalyst," *Catalysis Today*, vol. 232, pp. 89–98, 2014.
- [3] A. M. Abdullah, A. M. Mohammad, T. Okajima, F. Kitamura, and T. Ohsaka, "Effect of load, temperature and humidity on the pH of the water drained out from H₂/air polymer electrolyte membrane fuel cells," *Journal of Power Sources*, vol. 190, no. 2, pp. 264–270, 2009.
- [4] B. Braunschweig, D. Hibbitts, M. Neurock, and A. Wieckowski, "Electrocatalysis: a direct alcohol fuel cell and surface science perspective," *Catalysis Today*, vol. 202, pp. 197–209, 2013.
- [5] M. Bron and C. Roth, *Chapter 10-Fuel Cell Catalysis from a Materials Perspective New and Future Developments in Catalysis*, S. L. Suib, Ed., Elsevier, Amsterdam, Netherlands, 2013.
- [6] J. P. Stempien and S. H. Chan, "Comparative study of fuel cell, battery and hybrid buses for renewable energy constrained areas," *Journal of Power Sources*, vol. 340, pp. 347–355, 2017.
- [7] P. Y. You and S. K. Kamarudin, "Recent progress of carbonaceous materials in fuel cell applications: an overview," *Chemical Engineering Journal*, vol. 309, pp. 489–502, 2017.
- [8] S. Zhang, Y. Shao, G. Yin, and Y. Lin, "Facile synthesis of PtAu alloy nanoparticles with high activity for formic acid oxidation," *Journal of Power Sources*, vol. 195, no. 4, pp. 1103–1106, 2010.
- [9] I. M. Al-Akraa, A. M. Mohammad, M. S. El-Deab, and B. E. El-Anadouli, "Development of tailor-designed gold-platinum nanoparticles binary catalysts for efficient formic acid electrooxidation," *International Journal of Electrochemical Science*, vol. 7, no. 5, pp. 3939–3946, 2012.
- [10] M. S. El-Deab, A. M. Mohammad, G. A. El-Nagar, and B. E. El-Anadouli, "Impurities contributing to catalysis: enhanced electro-oxidation of formic acid at Pt/GC electrodes in the presence of vinyl acetate," *Journal of Physical Chemistry C*, vol. 118, no. 39, pp. 22457–22464, 2014.
- [11] G. A. El-Nagar, A. M. Mohammad, M. S. El-Deab, T. Ohsaka, and B. E. El-Anadouli, "Acrylonitrile-contamination induced enhancement of formic acid electro-oxidation at platinum nanoparticles modified glassy carbon electrodes," *Journal of Power Sources*, vol. 265, pp. 57–61, 2014.
- [12] I. M. Al-Akraa, "Efficient electro-oxidation of formic acid at Pd-MnO_x binary nanocatalyst: effect of deposition strategy," *International Journal of Hydrogen Energy*, vol. 42, no. 7, pp. 4660–4666, 2017.
- [13] M. S. El-Deab, G. A. El-Nagar, A. M. Mohammad, and B. E. El-Anadouli, "Fuel blends: enhanced electro-oxidation of formic acid in its blend with methanol at platinum nanoparticles modified glassy carbon electrodes," *Journal of Power Sources*, vol. 286, pp. 504–509, 2015.
- [14] A. M. Mohammad, G. A. El-Nagar, I. M. Al-Akraa, M. S. El-Deab, and B. E. El-Anadouli, "Towards improving the

- catalytic activity and stability of platinum-based anodes in direct formic acid fuel cells,” *International Journal of Hydrogen Energy*, vol. 40, no. 24, pp. 7808–7816, 2015.
- [15] Y. W. Rhee, S. Y. Ha, and R. I. Masel, “Crossover of formic acid through Nafion® membranes,” *Journal of Power Sources*, vol. 117, no. 1-2, pp. 35–38, 2003.
- [16] X. Wang, J.-M. Hu, and I.-M. Hsing, “Electrochemical investigation of formic acid electro-oxidation and its crossover through a Nafion® membrane,” *Journal of Electroanalytical Chemistry*, vol. 562, no. 1, pp. 73–80, 2004.
- [17] S. Hu, L. Scudiero, and S. Ha, “Electronic effect of Pd-transition metal bimetallic surfaces toward formic acid electrochemical oxidation,” *Electrochemistry Communications*, vol. 38, pp. 107–109, 2014.
- [18] A. M. Mohammad, S. Dey, K. K. Lew, J. M. Redwing, and S. E. Mohney, “Fabrication of cobalt silicide nanowire contacts to silicon nanowires,” *Journal of the Electrochemical Society*, vol. 150, no. 9, pp. G577–G580, 2003.
- [19] S. M. Dilts, A. Mohammad, K. K. Lew, and J. M. Redwing, “Mohney SE fabrication and electrical characterization of silicon nanowire arrays,” in *Proceedings of MRS Fall Meeting*, L. Tsybeskov, D. J. Lockwood, C. Delerue, and M. Ichikawa, Eds., pp. 287–292, Boston, MA, USA, November 2004.
- [20] D. Shir, B. Z. Liu, A. M. Mohammad, K. K. Lew, and S. E. Mohney, “Oxidation of silicon nanowires,” *Journal of Vacuum Science & Technology B: Microelectronics and Nanometer Structures*, vol. 24, no. 3, pp. 1333–1336, 2006.
- [21] A. M. Abdullah, T. Okajima, A. M. Mohammad, F. Kitamura, and T. Ohsaka, “Temperature gradients measurements within a segmented H₂/air PEM fuel cell,” *Journal of Power Sources*, vol. 172, no. 1, pp. 209–214, 2007.
- [22] G. A. El-Nagar and A. M. Mohammad, “Enhanced electrocatalytic activity and stability of platinum, gold, and nickel oxide nanoparticles-based ternary catalyst for formic acid electro-oxidation,” *International Journal of Hydrogen Energy*, vol. 39, no. 23, pp. 11955–11962, 2014.
- [23] J. K. Yoo and C. K. Rhee, “Formic acid oxidation on Bi-modified Pt surfaces: Pt deposits on Au versus bulk Pt,” *Electrochimica Acta*, vol. 216, pp. 16–23, 2016.
- [24] I. M. Al-Akraa, A. M. Mohammad, M. S. El-Deab, and B. E. El-Anadouli, “Electrooxidation of formic acid at platinum gold nanoparticle-modified electrodes,” *Chemistry Letters*, vol. 40, no. 12, pp. 1374–1375, 2011.
- [25] G. A. El-Nagar, A. M. Mohammad, M. S. El-Deab, and B. E. El-Anadouli, “Electrocatalysis by design: enhanced electrooxidation of formic acid at platinum nanoparticles-nickel oxide nanoparticles binary catalysts,” *Electrochimica Acta*, vol. 94, pp. 62–71, 2013.
- [26] G. Cabello, R.-rA. Davoglio, F. W. Hartl et al., “Microwave-assisted synthesis of Pt-Au nanoparticles with enhanced electrocatalytic activity for the oxidation of formic acid,” *Electrochimica Acta*, vol. 224, pp. 56–63, 2017.
- [27] L. Dai and S. Zou, “Enhanced formic acid oxidation on Cu-Pd nanoparticles,” *Journal of Power Sources*, vol. 196, no. 22, pp. 9369–9372, 2011.
- [28] L. Feng, J. Chang, K. Jiang et al., “Nanostructured palladium catalyst poisoning depressed by cobalt phosphide in the electro-oxidation of formic acid for fuel cells,” *Nano Energy*, vol. 30, pp. 355–361, 2016.
- [29] S. Li, D. Cheng, X. Qiu, and D. Cao, “Synthesis of Cu@Pd core-shell nanowires with enhanced activity and stability for formic acid oxidation,” *Electrochimica Acta*, vol. 143, pp. 44–48, 2014.
- [30] R. Ojani, Z. Abkar, E. Hasheminejad, and J.-B. Raouf, “Rapid fabrication of Cu/Pd nano/micro-particles porous-structured catalyst using hydrogen bubbles dynamic template and their enhanced catalytic performance for formic acid electro-oxidation,” *International Journal of Hydrogen Energy*, vol. 39, no. 15, pp. 7788–7797, 2014.
- [31] G. Chen, M. Liao, B. Yu et al., “Pt decorated PdAu/C nanocatalysts with ultralow Pt loading for formic acid electrooxidation,” *International Journal of Hydrogen Energy*, vol. 37, no. 13, pp. 9959–9966, 2012.
- [32] Y.-H. Qin, Y. Jiang, D.-F. Niu et al., “Carbon nanofiber supported bimetallic PdAu nanoparticles for formic acid electrooxidation,” *Journal of Power Sources*, vol. 215, pp. 130–134, 2012.
- [33] I. M. Al-Akraa, A. M. Mohammad, M. S. El-Deab, and B. E. El-Anadouli, “Electrocatalysis by design: synergistic catalytic enhancement of formic acid electro-oxidation at core-shell Pd/Pt nanocatalysts,” *International Journal of Hydrogen Energy*, vol. 40, no. 4, pp. 1789–1794, 2015.
- [34] Y. Jin, J. Zhao, F. Li et al., “Nitrogen-doped graphene supported palladium-nickel nanoparticles with enhanced catalytic performance for formic acid oxidation,” *Electrochimica Acta*, vol. 220, pp. 83–90, 2016.
- [35] F. Gopal and R. Arab, “A preliminary study of the electrocatalytic reduction of oxygen on Cu–Pd alloys in alkaline solution,” *Journal of Electroanalytical Chemistry*, vol. 647, no. 1, pp. 66–73, 2010.
- [36] F. Wang and G. Lu, “Hydrogen feed gas purification over bimetallic Cu–Pd catalysts – effects of copper precursors on CO oxidation,” *International Journal of Hydrogen Energy*, vol. 35, no. 13, pp. 7253–7260, 2010.
- [37] P. Mani, R. Srivastava, and P. Strasser, “Dealloyed binary PtM₃ (M=Cu, Co, Ni) and ternary PtNi₃M (M=Cu, Co, Fe, Cr) electrocatalysts for the oxygen reduction reaction: performance in polymer electrolyte membrane fuel cells,” *Journal of Power Sources*, vol. 196, no. 2, pp. 666–673, 2011.
- [38] G. A. El-Nagar, A. M. Mohammad, M. S. El-Deab, and B. E. El-Anadouli, “Propitious dendritic Cu₂O-Pt nanostructured anodes for direct formic acid fuel cells,” *ACS Applied Materials & Interfaces*, vol. 9, no. 23, pp. 19766–19772, 2017.
- [39] G. A. El-Nagar, A. M. Mohammad, M. S. El-Deab, and B. E. El-Anadouli, “Facilitated electro-oxidation of formic acid at nickel oxide nanoparticles modified electrodes,” *Journal of The Electrochemical Society*, vol. 159, no. 7, pp. F249–F254, 2012.
- [40] T. Teranishi and M. Miyake, “Size control palladium nanoparticles and their crystal structures,” *Chemistry of Materials*, vol. 10, no. 2, pp. 594–600, 1998.
- [41] B. Zhang, D. Ye, J. Li, X. Zhu, and Q. Liao, “Electrodeposition of Pd catalyst layer on graphite rod electrodes for direct formic acid oxidation,” *Journal of Power Sources*, vol. 214, pp. 277–284, 2012.
- [42] F. Alardin, H. Wullens, S. Hermans, and M. Devillers, “Mechanistic and kinetic studies on glyoxal oxidation with Bi- and Pb-promoted Pd/C catalysts,” *Journal of Molecular Catalysis A: Chemical*, vol. 225, no. 1, pp. 79–89, 2005.
- [43] L. Lu, L. Shen, Y. Shi et al., “New insights into enhanced electrocatalytic performance of carbon supported Pd-Cu catalyst for formic acid oxidation,” *Electrochimica Acta*, vol. 85, pp. 187–194, 2012.
- [44] J.-H. Choi, K.-J. Jeong, Y. Dong et al., “Electro-oxidation of methanol and formic acid on PtRu and PtAu for direct liquid

- fuel cells,” *Journal of Power Sources*, vol. 163, no. 1, pp. 71–75, 2006.
- [45] S. M. Baik, J. Han, J. Kim, and Y. Kwon, “Effect of deactivation and reactivation of palladium anode catalyst on performance of direct formic acid fuel cell (DFAFC),” *International Journal of Hydrogen Energy*, vol. 36, no. 22, pp. 14719–14724, 2011.
- [46] L. Wang, J.-J. Zhai, K. Jinag, K.-Q. Wang, and W.-B. Cai, “Pd-Cu/C electrocatalysts synthesized by one-pot polyol reduction toward formic acid oxidation: structural characterization and electrocatalytic performance,” *International Journal of Hydrogen Energy*, vol. 40, no. 4, pp. 1726–1734, 2015.
- [47] J. Jiang and A. Kucernak, “Electrooxidation of small organic molecules on mesoporous precious metal catalysts: CO and methanol on platinum,” *Journal of Electroanalytical Chemistry*, vol. 533, no. 1-2, pp. 153–165, 2002.
- [48] M. Osawa, K. Komatsu, G. Samjeske et al., “The role of bridge-bonded adsorbed formate in the electrocatalytic oxidation of formic acid on platinum,” *Angewandte Chemie International Edition*, vol. 50, no. 5, pp. 1159–1163, 2011.
- [49] I. M. Al-Akraa, A. M. Mohammad, M. S. El-Deab, and B. E. El-Anadouli, “Electrocatalysis by nanoparticle: enhanced electro-oxidation of formic acid at NiO_x-Pd binary nanocatalysts,” *Journal of The Electrochemical Society*, vol. 162, no. 10, pp. F1114–F1118, 2015.
- [50] I. M. Al-Akraa, A. M. Mohammad, M. S. El-Deab, and B. E. El-Anadouli, “Advances in direct formic acid fuel cells: fabrication of efficient Ir/Pd nanocatalysts for formic acid electro-oxidation,” *International Journal of Electrochemical Science*, vol. 10, no. 4, pp. 3282–3290, 2015.



Hindawi
Submit your manuscripts at
www.hindawi.com

